Journal of Hydroscience and Hydraulic Engineering
Vol. 7, No. 1, November, 1989, pp.1-11

OBSERVATIONS AND SIMULATION OF RAINFALL IN MOUNTAINOUS AREAS

By

K. TATEYA, Executive Director
Foundation of Hokkaido River Disaster Prevention Research Center
Sapporo, Japan

M. NAKATSUGAWA, Research Engineer
Civil Engineering Research Institute, Hokkaido Development Bureau
Sapporo, Japan

and

T. YAMADA, Associate Professor
Department of Civil Engineering, Hokkaido University
Sapporo, Japan

SYNOPSIS

In this paper, the results of the field observation of rainfall carried out by the authors are shown and the effects of height or direction of the mountain on rainfall are discussed. With these investigations, we calculate the wind field in mountainous areas, which is estimated as the potential flow by using the digital maps and spectral analysis. Combining the calculated wind field with the Kessler model for rainfall, we simulate the rainfall field in the mountainous areas. Comparing the observed data with the calculated rainfall pattern, we confirm that the above-mentioned calculation can precisely simulate the actual orographic effect on rainfall fields. In addition, an attempt is made to transform the three-dimensional model to the two-dimensional one, to reduce the computational burden for practical applications. Combining the physically-based model with the Radar information, we intend to propose the spatial and time-sequential rainfall forecast method. Such rainfall forecast information might be utilized for the flood forecast using the distributed run-off model.

1. INTRODUCTION

The observation and forecast of heavy rainfall is very important for the purpose of disaster prevention. The Japanese Ministry of Construction intends to cover the whole country by 22 radar stations. Such a radar network system will supply the information on temporal and spatial distributions of rainfall. The simulation model coupled with the observed data from radar is of practical use to forecast the rainfall accurately. Many researchers have suggested that the occurrences of heavy rainfall are often connected with the orographic conditions. However, it is extremely difficult to verify the orographic effects, because there are few raingauge stations in mountainous areas. Therefore, it is required to develop the model which can estimate and forecast heavy rainfall in such areas. The meteorological investigations connected with the orographic rainfall have been carried out by Scorer (1949)(4), Sarker (1967)(5), Colton (1976)(6), Tatehira (1976)(7), Sawyer (1952 and 1956) (8)(9) and Gocho (1978)(10). In the present paper, the results of the field observations by the authors are shown from the topographical point of view. On the other hand, we calculate the rainfall field by the numerical method and obtain some knowledge about the characteristics of orographic rainfall(14).

2. FIELD OBSERVATIONS OF OROGRAPHIC RAINFALL

2—1 Previous studies by Kikuchi et al.(1978 and 1981) (1)(2)(3)

Kikuchi et al. carried out the observations of rainfall amounts using a special raingauge network along the slope in the Orofure mountain range. The Orofure mountain range is located in the south-west part of Hokkaido Island, Japan as shown in Fig. 2.1 and is famous for occurrences of heavy rainfall. From the results of their investigations, they have suggested that when the humid south-easterly wind from the Pacific Ocean prevails on the wall-like Orofure mountain range, the strong ascending draft is generated along the south-east slope of the ridge and such a condition is important as a direct trigger of heavy rainfall in this area. Furthermore, the orographic rainfall is classified into "continuous type" generated by the upglide of a humid air mass on the slope and "convective type" influenced by the atmospheric disturbance in the synoptic scale. A series of their observations indicate that the ratio of rainfall amount of the mountainous region to the seaside region in the case of the former is larger than that in the case of the latter. It shows that the orographic effect remarkably appears in the case of "continuous type" rainfall.

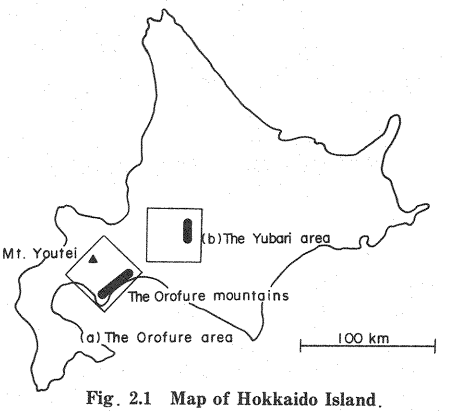

Fig. 2.1 Map of Hokkaido Island.

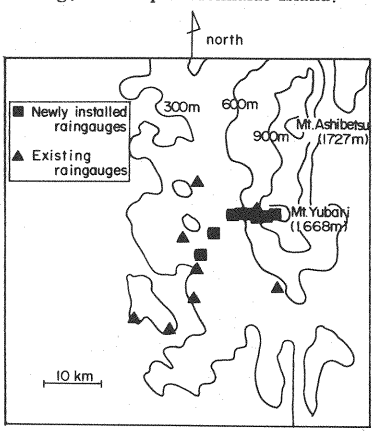

Fig. 2.2 Location of raingauges installed in the Yubari area.

2—2 Field observations carried out by the authors

Fig. 2.1 (Fig. 2.2 in detail) also shows the area around Mt. Yubari which is located in the central part of Hokkaido Island. There is the mountain range stretching from the south to the north in this area. We installed 10 raingauges (square marks as shown in Fig. 2.2) along the west slope in Mt. Yubari in cooperation with the Ishikari River Local Head Office, Hokkaido Development Bureau and we carried out the special observation of rainfall from 20 July, 1988 to 15 October, 1988. In addition, we use data obtained from 8 existing raingauges (triangle marks as shown in Fig. 2.2). During our observations, we could fortunately observe the heavy rainfall on 25 and 26 August, 1988. The synoptic situations in this period showed that the humid airflow from tropical cyclone in the Pacific Ocean and

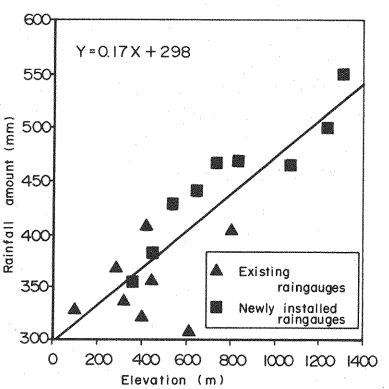

Fig. 2.3 Observed rainfall amount with elevation (from 20 July to 15 October, 1988)

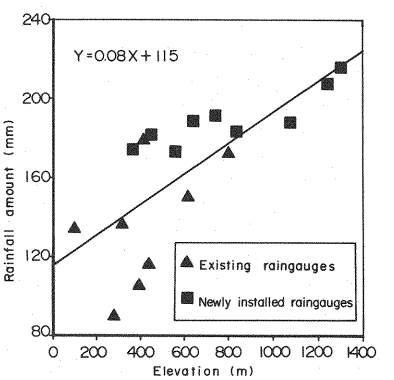

Fig. 2.4 Observed rainfall amount with elevation (from 25 August to 31 August, 1988)

the cold airflow from the Eurasian Continent prevailed on Hokkaido and the stationary front grew remarkably. Along the west slope of Mt. Yubari, the largest rainfall intensity during that period was observed in the morning of 26 August, when the wind direction changed from westerly to easterly in connection with the movement of a front. Figs. 2.3 and 2.4 illustrate the obtained important results. Fig. 2.3 shows the behavior of the total rainfall amounts with the elevation in the whole observation period (7/20～10/15, 1988), while Fig. 2.4 shows the amounts during a week (8/25～8/31, 1988) which includes the event of the above-mentioned heavy rainfall. These examples show that the total amount of rainfall on the slope of the mountain increases linearly with the elevation. Furthermore, it follows from Figs. 2.3 and 2.4 that the rainfall at the highest site is nearly twice that at the lowest site (1000 m difference between 2 sites). The rainfall pattern is not necessarily regular for the cases where convective instability might take place under the large disturbance. However, the behavior of the accumulated rainfall amount with elevation shows clearly the typical orographic effect during the weekly or monthly periods.

3. MODELLING OF THE WIND FIELD IN A MOUNTAINOUS AREA

3—1 Calculation method

In the previous studies, the Scorer equation has been often used to calculate the airflow over the mountains. In this paper, the typical orographic effect on the wind field is considered, assuming that the

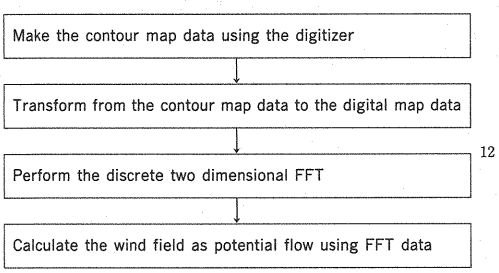

Fig. 3.1 Flow chart for calculation of the wind field.

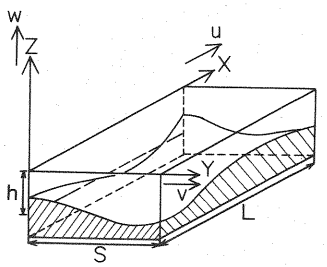

Fig. 3.2 Coordinate system for calculation

Table 3.1 Basic equations for calculation of the wind field

Three-dimensional Laplace equation

$$\frac{\partial^2\phi}{\partial x^2}+\frac{\partial^2\phi}{\partial y^2}+\frac{\partial^2\phi}{\partial z^2}=0 \qquad (3.\ 1)$$

Velocity potential

$$\phi=Ux+\phi(z)\cdot e^{ikx}\cdot e^{ily} \qquad (3.\ 2)$$

Topographic function

$$\eta=-h+a\cdot e^{ikx}\cdot e^{ily} \qquad (3.\ 3)$$

Boundary condition

$$\frac{\partial\phi}{\partial z}=0 \qquad at\quad z=0 \qquad (3.\ 4)$$

$$\frac{\partial\phi}{\partial z}=U\cdot\frac{\partial\eta}{\partial x} \qquad at\quad z=-h \qquad (3.\ 5)$$

Solutions of windspeed

$$u=U+U\frac{1}{N^2}\sum_{p=0}^{N-1}\sum_{q=0}^{N-1}F(p,q)\frac{k^2\cdot\cosh(\beta z)}{\beta\cdot\sinh(\beta h)}\exp\left(\frac{2\pi i}{N}mp\right)\exp\left(\frac{2\pi i}{N}nq\right) \qquad (3.\ 6)$$

$$v=U\frac{1}{N^2}\sum_{p=0}^{N-1}\sum_{q=0}^{N-1}F(p,q)\frac{k\cdot l\cdot\cosh(\beta z)}{\beta\cdot\sinh(\beta h)}\exp\left(\frac{2\pi i}{N}mp\right)\exp\left(\frac{2\pi i}{N}nq\right) \qquad (3.\ 7)$$

$$w=-U\frac{1}{N^2}\sum_{p=0}^{N-1}\sum_{q=0}^{N-1}F(p,q)\frac{k\cdot i\cdot\sinh(\beta z)}{\sinh(\beta h)}\exp\left(\frac{2\pi i}{N}mp\right)\exp\left(\frac{2\pi i}{N}nq\right) \qquad (3.\ 8)$$

where

u, v, w ; *Windspeeds in x, y and z directions* ($m\ sec^{-1}$)
U ; *Windspeed of main stream* ($m\ sec^{-1}$)
$-h$; *Averaged altitude of the ground surface* ($m\ sec^{-1}$)
$\phi(z)$; *Velocity potential in z direction* ($m^2\ sec^{-1}$)
k, l ; *Horizontal wave number* ($\beta=\sqrt{k^2+l^2}$)
N ; *Number of FFT terms*
$F(p,q)$; *FFT component*

atmosphere is saturated and has an undisturbed and steady uniform flow. Additionally, it is assumed that the airflow which contributes to rainfall generation has the larger inertia, comparing with topographical fluctuations and the Coriolis effect is assumed to be negligible in the scale from the geodynamical point of view. According to the above assumptions, we adopt the potential flow for modelling the wind field(12). Fig. 3.1 shows the flow-chart for calculation of the wind field. After any contour line on the map of a basin is transformed to the gridpoint data of surface elevation (the digital map data), the two-dimensional discrete Fourier Transform for these digital map data is conducted. Using those FFT data, the three components of windspeed are obtained as the solutions of the three-dimensional Laplace equation as shown in Table 3.1. The coordinate system for calculation is depicted in Fig. 3.2.

3—2 Topographical effects on wind field

To understand how the mountain shapes exert influence on the ascending wind along the slope, we

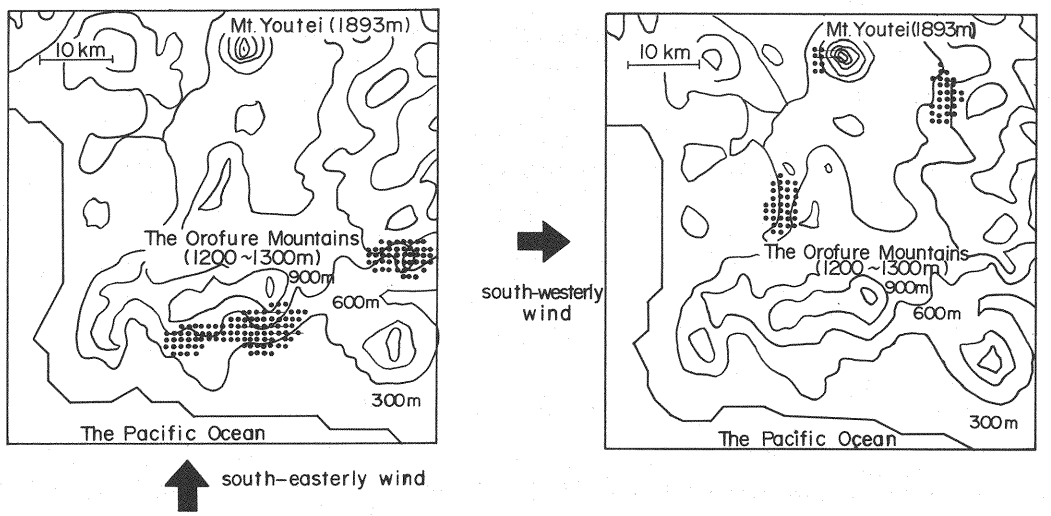

(a) the case of south-easterly wind (b) the case of south-westerly wind

Fig. 3.3 The area of strong ascending wind (The Orofure area)

calculated the wind field shown in (a) the Orofure area and (b) the Yubari area of Fig. 2.1. The computational domain covers 10 km in the altitude and 63 km in the horizontal square area. The grid sizes are 1 km in the horizontal directions x and y and 0.2 km in the vertical direction z. The Orofure area includes the Orofure mountains with elevation of 1200~1300 m which extends in a northeast to southwest direction along the Pacific Ocean and Mt. Youtei with the height of 1893 m which has an isolated peak. In the Yubari area, there are the mountain range at the elevation of 1600~1700 stretching from the south to the north. The dotted parts of Figs. 3.3 and 3.4 show the areas where the strong ascending windspeeds more than 2% of the main stream

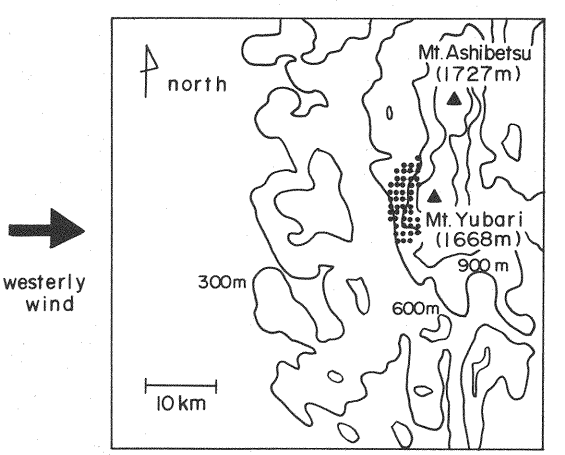

Fig. 3.4 The area of strong ascending wind (The Yubari area)

at the altitude of 5000 m are calculated. The main stream windspeed of 10 m/s is assumed in each case as the boundary condition. In the case of south-easterly wind in the Orofure area, the ascending wind is strong at the upper height above the south-east slope of the Orofure mountain range, which is caused by the existence of the wall-like slope, as shown in Fig. 3.3 (a). This figure also shows that, around an isolated mountain like Mt. Youtei, the ascending wind is not so strong, because of the so-called evading effect of the wind in spite of a higher altitude of it. Fig. 3.3 (b) shows that the south-westerly wind cannot form wider and stronger ascending wind field than the south-easterly one which attack to the wall of the mountain range. Fig. 3.4 clearly shows that the ascending wind field is formed above the west slope of Mt. Yubari where we installed some raingauges.

4. ANALYSIS OF OROGRAPHIC RAINFALL FIELD

4—1 Model of rainfall

In this study, three-dimensional model of liquid water mass with Kessler's parameterization(11)(13) is adopted to calculate the rainfall field, combined with the calculated wind field. Fig. 4.1 illustrates the schematic description of rainfall mechanism in the Kessler model. The liquid water mass is separated into cloud water and raindrops based on the size of water drops. The fundamental equations are summarized in Table 4.1. Equations (4.1) and (4.2) are the conservation equations for cloud water and raindrops. The parameters used in these equations are decided by considering the micro-physics of liquid water mass in which the thermodynamical processes are taken into account. Both equations are solved numerically by a finite difference method using the same three-dimensional computational grid as in the wind calculation. The computational domain covers 10 km in altitude and 63 km in the horizontal square area. The size of each grid is 1km in x and y directions, and 0.2km in z direction. The time step (Δt) for the

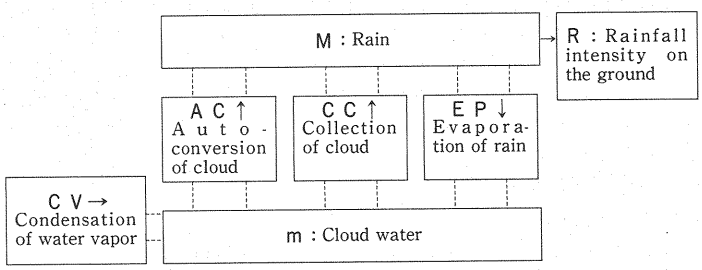

Fig. 4.1 Rainfall mechanism in the kessler model

Table 4.1 Basic equations for three-dimensional calculation of the rainfall field.

$$\frac{\partial m}{\partial t} = -u\frac{\partial m}{\partial x} - v\frac{\partial m}{\partial y} - w\frac{\partial m}{\partial z} - AC - CC + EP + CV \quad (4.1)$$

$$\frac{\partial M}{\partial t} = -u\frac{\partial M}{\partial x} - v\frac{\partial M}{\partial y} - (w+V)\frac{\partial M}{\partial z} + AC + CC - EP \quad (4.2)$$

$$AC = K_1(m-a) \quad (m>a)$$
$$= 0 \quad (m<a) \quad (4.3)$$

$$CC = 6.96\times10^{-4}\cdot E\cdot No^{1/8}\cdot m\cdot M^{7/8}\cdot exp(k\cdot z/2) \quad (4.4)$$

$$EP = 1.93\times10^{-6}\cdot No^{7/20}\cdot m\cdot M^{13/20} \quad (4.5)$$

$$CV = w\cdot(A+B\cdot z) \quad (4.6)$$

$$V = -38.3\,No^{-1/8}M^{1/8}exp(k\cdot z/2) \quad (4.7)$$

$$R = 138\,No^{-1/8}M^{9/8} \quad (4.8)$$

where

- m ; *Cloud water content* ($g\ m^{-3}$)
- M ; *Rain water content* ($g\ m^{-3}$)
- u,v,w ; *Windspeeds in x, y and z directions* ($m\ sec^{-1}$)
- AC ; *Auto-conversion of cloud* ($g\ m^{-3}\ sec^{-1}$)
- CC ; *Collection of cloud* ($g\ m^{-3}\ sec^{-1}$)
- EP ; *Evaporation of rain* ($g\ m^{-3}\ sec^{-1}$)
- CV ; *Condensation of water vapor* ($g\ m^{-3}\ sec^{-1}$)
- V ; *Fallspeed of raindrops* ($m\ sec^{-1}$)
- R ; *Rainfall rate* ($mm\ h^{-1}$)
- K_1 ; *Constant* ($=10^{-3}\ sec^{-1}$)
- a ; *Threshold value of auto-conversion* ($=0.5\ g\ m^{-3}$)
- E ; *Collection efficiency* ($=1$)
- No ; *Marshall-Palmer constant* ($=10^{7}m^{-4}$)
- k ; *Lapse rate of air density* ($=10^{-4}m^{-1}$)
- z ; *Altitude* (m)
- A ; *Constant* ($=3\times10^{-3}g\ m^{-4}$)
- B ; *Constant* ($=-3\times10^{-7}g\ m^{-5}$)

numerical calculation is decided from the following condition.

$$\Delta t < \mathrm{Min}\left[\left| \frac{\Delta x}{u} \right|, \left| \frac{\Delta y}{v} \right|, \left| \frac{\Delta z}{w} \right| \right]$$

The boundary conditions of m and M are as follows :

$\frac{\partial m}{\partial x} = 0$, $\frac{\partial \mathrm{M}}{\partial x} = 0$ at the edge points of x direciton.

$\frac{\partial m}{\partial y} = 0$, $\frac{\partial \mathrm{M}}{\partial \mathrm{y}} = 0$ at the edge points of y direction.

$m = 0$, $\mathrm{M} = 0$ at the points on the ground surface of z direction.

$m = 0$, $\mathrm{M} = 0$ at the points on the upper boundary of z direction.

These calculations are performed under some assumptions, such as steady wind field, the Marshall-Palmer distribution in microphysical parameters and a constant terminal velocity as fallspeed of raindrops. Saturated air is assumed as the initial condition (m=0) everywhere. Convective instability induced from thermodynamical processes should be considered to fully explain the rainfall mechanism. However, in this study, we investigate the basic mechanism of rainfall caused by the topographical effects and deal with the stratiform rainfall. Therefore, the storm rainfall as caused by convective instability is not considered.

4—2 Basic characteristics of calculated rainfall using the Kessler model

In order to understand the characteristics of rainfall simulated by the Kessler model, some numerical experiments are carried out for the simply shaped topography. The obtained results are summarized as follows :

1) Steady characteristics of rainfall

The calculated rainfall amount and its spatial distribution reach the steady state in 30 or 40 minutes. When we decrease the threshold value of auto-conversion (a in Eq. (4.3)), the raindrops from the cloud water are quickly formed and the rainfall field reach the steady state promptly.

2) Advection effects

Fig. 4.2 shows the calculated results for some cases of uniform windspeed around a concentric circular peaked mountain. It is recognized from this figure that the larger the main stream windspeed is, the stronger the rainfall intensity is, because the ascending windspeed increases. However, when the horizontal advection velocity increases excessively, the rainband shifts to the lee side and the rainfall intensity decreases beyond some threshold value.

3) Condensation of cloud water from water vapor

To investigate the effect of condensation on rainfall, some different values of the condensation term (Eq. (4.6)) are used in the calculation. Fig. 4.3 shows the distribution of the rainfall intensity calculated along the line of wind direction passing through the summit of the concentric circular peaked mountain. The values of the condensation term are directly proportional to the ascending windspeeds. The result clearly shows that the rainfall intensity is linearly propotional to the ascending windspeed in the condensation term.

4) Mountain shape

To investigate the topographic effect on rainfall, especially mountain shapes, two typical cases are considered ; the concentric circular peaked shape and two-dimensional wall-like shape with the same elevation. Fig. 4.4 shows the calculated rainfall intensity along the line of wind direction passing through the summit (the same cross sectional shape). From this figure, it is recognized that the ascending wind with or without the evading effects directly influence the rainfall intensity. Such topographic effects can be thought of as an important factor on the actual rainfall field.

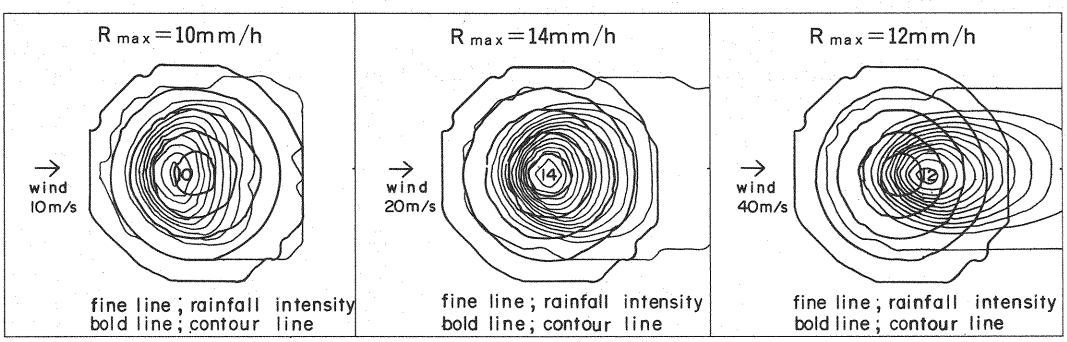

a) 10 m/s b) 20 m/s c) 40 m/s

Fig. 4.2 The rainband calculated with different main stream windspeed.

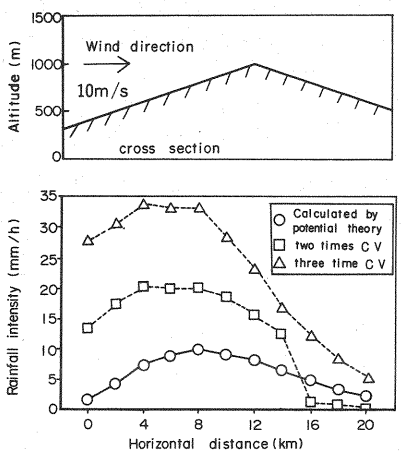

Fig. 4.3 Rainfall intensity calculated with the different ascending wind in the condensation term (CV)
(along the line through the summit in a concentric circular mountain)

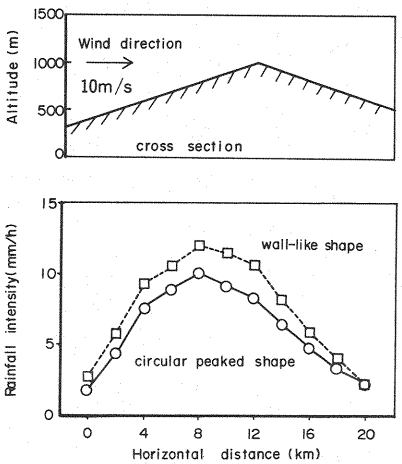

Fig. 4.4 Rainfall intensity calculated with the different topographic shape
(along the line through the summit)

4—3 Calculated results on actual topography

Fig. 4.5 (a) shows the contour lines of rainfall intensity calculated in the Orofure area where the south-easterly wind is prevailing. The windspeed of main stream is 10m/s and saturated air is given as the initial condition. The calculated result shows the same tendency as the observation results performed by Kikuchi et al., i.e., typical rainband is formed along the south-east slope of the Orofure mountains. The simulated rainfall intensity at the center of rainband is about 10mm/h. However, the actual heavy rainfall recorded in this area contained the rainfall intensity higher than 50 mm/h. Therefore, the calculated rainfall amount is underestimated, because the above-mentioned simulation considers only the stratiform rainfall due to the typical orographic effect. In the case of the south-westerly wind, only a half intensity of rainfall is calculated, compared with the case of south-easterly wind as shown in Fig. 4.5 (b). These results clearly show the effect of mountain shapes on rainfall amount and distribution. Fig. 4.6 shows the rainfall contour lines calculated in the Yubari area where the westerly wind are predominant. The result illustrates that the typical rainband is formed by the presence of the wall-like mountain range as described in the previous example.

Furthermore, Fig. 4.7 shows the change of the rainfall intensity with the elevation at the nearest computational grid point where the raingauge shown in Fig. 2.2 was installed. It can be recognized from Fig. 4.7 that the calculated results are favorably compared with the observed rainfall amount which increases linearly with the elevation (refer to Figs. 2.3 and 2.4).

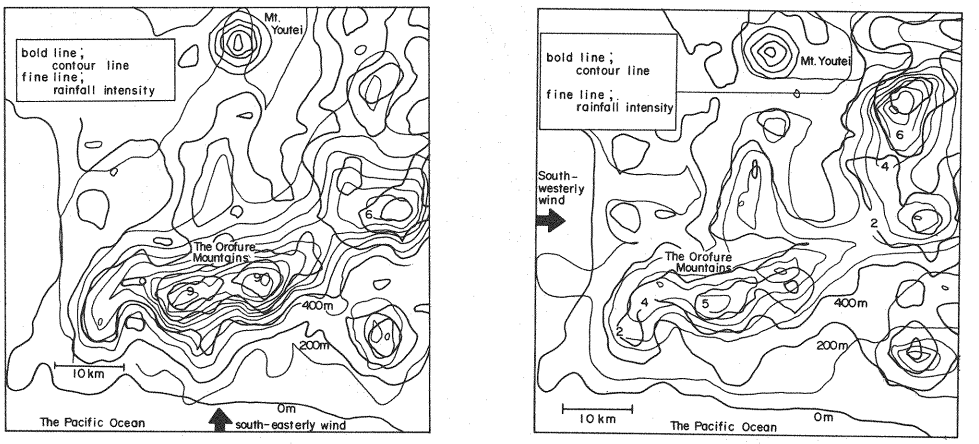

a) The case of south−easterly wind　　b) The case of south−westerly wind

Fig. 4.5 Calculated rainfall intensity (The Orofure area)

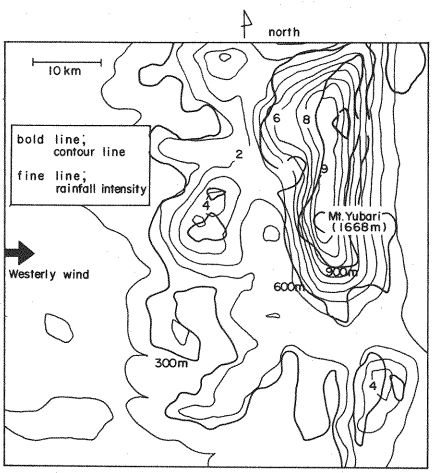

Fig. 4.6 Calculated rainfall intensity (The Yubari area)

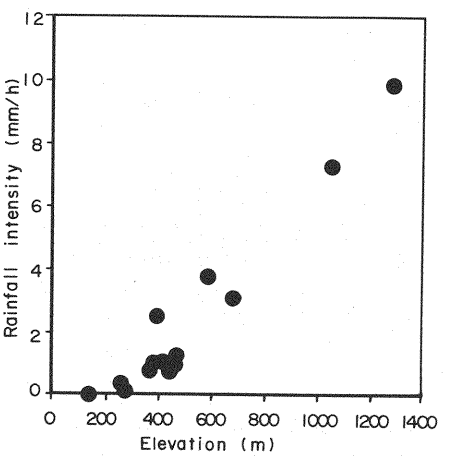

Fig. 4.7 Calculated rainfall intensity with elevation (The Yubari area)

4—4 Effects of topographic scale on rainfall

As mentioned previously, the present calculation method utilizes the FFT data of the digital map to obtain the wind field numerically. Fig. 4.8 shows a spectrum of the FFT components for the Orofure area. In order to understand the scale effects of topography on rainfall, we removed high frequency terms larger than the 10th term of FFT, which correspond to the scales less than 5 km in the actual topography according to the sampling theorem. We carried out a series of recalculations using a topography without those high frequency components. The calculated rainfall field under the south-easterly wind in the Orofure area is shown in Fig.

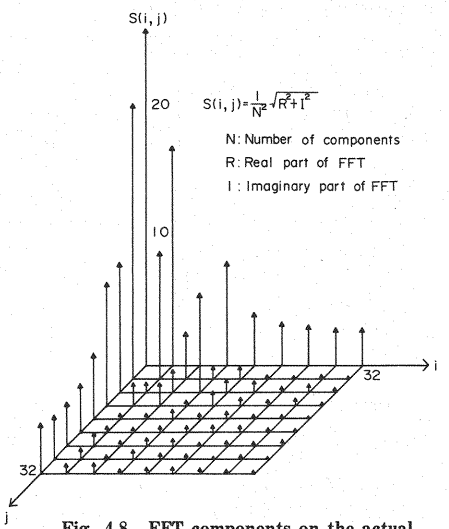

Fig. 4.8 FFT components on the actual topography (The Orofure area)

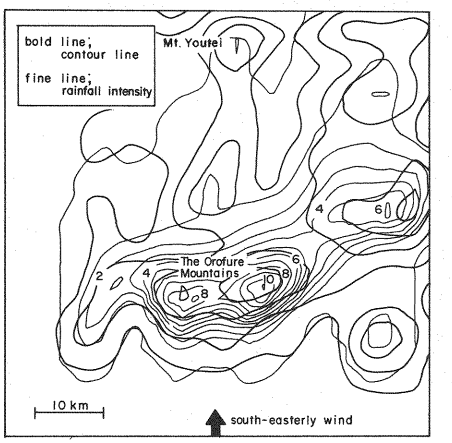

Fig. 4.9 Calculated rainfall intensity (high frequency components of FFT are removed, The Orofure area)

4.9. The obtained result demonstrates the same tendency of rainbands as that in Fig. 4.5 (a). It is understood from this figure that the scales less than 5 km have no significant effects on orographic rainfall pattern.

4—5 Two dimensional modelling of rainfall

Calibration and computational efforts are too stringent in the practical application of a three-dimensional rainfall model. For the purpose of real-time rainfall forecasting using radar information, the two-dimensional model is of practical use to reduce computer storage and time. Hence an attempt is made to transform the three-dimensional model to the two-dimensional one by integrating and averaging relevant variables and parameters in the vertical direction. In this operation, the basic equations are averaged vertically, assuming that cloud and rainfall amounts are uniform in each vertical column. In this section, it is confirmed that the rainfall field calculated by the three-dimensional model are simulated by the simplified one. The basic equations for this calculation are given in Table 4.2. These equations are solved numerically using the finite difference method and a series of calculations for rainfall are performed under the same conditions as for the three-dimensional one. The wind components in the equations are obtained by averaging the solutions of the three-dimensional potential flow vertically.

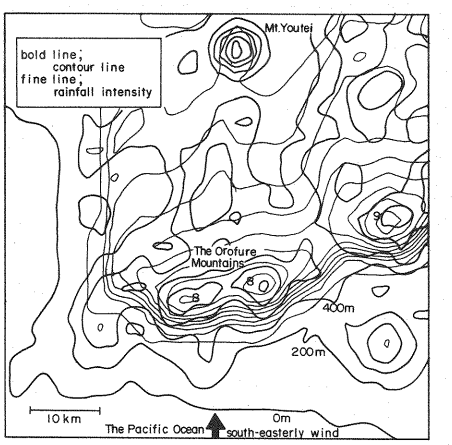

Fig. 4.10 Calculated rainfall intensity using two-dimensional model (The Orofure area)

First, the rainfall fields are calculated on the wall-like as well as concentric circular peaked shapes of the mountain as done in the numerical experiments using the three-dimensional model. The rainfall pattern in the former case bears out the similar tendency as the results obtained from use of the three-dimensional method.

Table 4.2 Basic equations for two-dimensional calculation of the rainfall field

$$\frac{\partial \overline{m}}{\partial t} = -\overline{u}\frac{\partial \overline{m}}{\partial x} - \overline{v}\frac{\partial \overline{m}}{\partial y} - \frac{\overline{u}\,\overline{m}}{H-h}\frac{\partial h}{\partial x} - \frac{\overline{v}\,\overline{m}}{H-h}\frac{\partial h}{\partial y} - \overline{AC} - \overline{CC} + \overline{EP} + \overline{CV} \quad (4.9)$$

$$\frac{\partial \overline{M}}{\partial t} = -\overline{u}\frac{\partial \overline{M}}{\partial x} - \overline{v}\frac{\partial \overline{M}}{\partial y} + \frac{\overline{V}\,\overline{M}}{H-h} - \frac{\overline{u}\,\overline{M}}{H-h}\frac{\partial h}{\partial x} - \frac{\overline{v}\,\overline{M}}{H-h}\frac{\partial h}{\partial y} + \overline{AC} + \overline{CC} - \overline{EP} \quad (4.10)$$

$$\overline{AC} = K_1(\overline{m}-a) \quad (\overline{m}>a), \qquad = 0 \quad (\overline{m}<a) \quad (4.11)$$

$$\overline{CC} = 6.96\times10^{-4} E No^{1/8}\overline{m}\,\overline{M}^{7/8} \quad (4.12)$$

$$\overline{EP} = 1.93\times10^{-6} No^{7/20}\overline{m}\,\overline{M}^{13/20} \quad (4.13)$$

$$\overline{CV} = \overline{w}\left\{A+\frac{B}{2}(H+h)\right\} \quad (4.14)$$

$$\overline{V} = -38.3\, No^{-1/8}\overline{M}^{1/8} \quad (4.15)$$

where

- $\overline{m}$; *Vertically averaged cloud water content* ($g\ m^{-3}$)
- $\overline{M}$; *Vertically averaged rain water content* ($g\ m^{-3}$)
- $\overline{u},\overline{v},\overline{w}$; *Vertically averaged windspeeds in x, y and z directions* ($m\ sec^{-1}$)
- $\overline{AC}$; *Vertically averaged auto-conversion of cloud* ($g\ m^{-3}sec$)
- $\overline{CC}$; *Vertically averaged collection of cloud* ($g\ m^{-3}sec$)
- $\overline{EP}$; *Vertically averaged evaporation of rain* ($g\ m^{-3}sec$)
- $\overline{CV}$; *Vertically averaged condensation of water vapor* ($g\ m^{-3}\ sec$)
- $\overline{V}$; *Vertically averaged fallspeed of raindrops* ($m\ sec^{-1}$)
- H ; *Altitude of upper boundary layer* (m)
- h ; *Elevation of the ground surface* (m)
- K_1 ; *Constant* ($=10^{-3}sec^{-1}$)
- a ; *Threshold value of auto-conversion* ($=0.5\ g\ m^{-3}$)
- E ; *Collection efficiency* ($=1$)
- No ; *Marshall-Palmer constant* ($=10^7 m^{-4}$)
- A ; *Constant* ($=3\times10^{-3} g\ m^{-4}$)
- B ; *Constant* ($=-3\times10^{-7} g\ m^{-5}$)

However, in the latter case, the simulated rainbands shift to the lee side in comparison with the three-dimensional simulation, because of the horizontal advection effect emphasized excessively. Accordingly, the two-dimensional model fails to produce the evading effect of wind around a mountain. The vertical wind component influenced by the topography is one of the significant factors on rainfall fields. Therefore, the ascending wind velocity must be estimated precisely. Numerical experiments of rainfall for the actual topography are conducted in the case of south-easterly wind in the Orofure area as shown in Fig. 4.10. The reproduced synoptic rainfall field shows the same pattern as the result of the three-dimensional simulation (compare with Fig. 4.5). Even the simplified version can reproduce the heavy rainfall along the wall-like slope of the Orofure mountain range. It follows from these calculations that the two-dimensional model proposed herein offers considerable promise for practical use.

5. CONCLUSIONS

On the basis of the field observations and analysis for rainfall field in mountainous areas, the results are briefly summarized as follows:

1) The observed data clearly show that rainfall amounts on the slope of the mountain increase linearly with the elevation increasing. Such orographic effects of rainfall can be reproduced by the simulation method combined the Kessler model with the potential flow for the wind components.

2) When the humid wind blows to the wall-like mountains, the heavy rainfall is observed along the slope which faces the wind direction and such effect connected with the mountain shape is also confirmed by the above-mentioned simulation.

3) When the ascending wind in the condensation term is stronger, the amount of rainfall increases linearly. On the other hand, when the horizontal advection effect is in excess, the rainfall intensity decreases.

4) No significant effects of the distribution and the amount of rainfall are discerned, even when high frequency components of FFT (i.e., the topographic scale in the horizontal directions is less than 5 km) are neglected.

5) The simplified two-dimensional model can operationally simulate the same synoptic rainfall field as by the three-dimensional one.

ACKNOWLEDGEMENTS

The authors wish to express their great appreciation to Prof. Fujita and Dr. Hoshi who gave us many invaluable suggestions and comments. Thanks are also due to the flood forecasting section, the Ishikari River Local Head Office, Hokkaido Development Bureau which cooperates for the field observations and offers many data and materials.

REFERENCES

1. Takeda, E. and Kikuchi, K. : Local Heavy Rainfalls in Hokkaido Island, Japan (1), Geophysical Bulletin of Hokkaido University, Sapporo, Japan, Vol.37, pp.19−29, 1978. (in Japanese)

2. Konno, T. and Kikuchi, K. : Properties of Local Heavy Rainfall on the Southeast Slope of Orofure Mountain Range in the Iburi District, Hokkaido, Japan (1), Geophysical Bulletin of Hokkaido University, Sapporo, Japan, Vol.39, pp.1−18, 1981. (in Japanese)

3. Kikuchi, K., Harimaya, T. and Horie, N. : Analyses of the Properties of Local Heavy Rainfall in the Southwestern Part of Hokkaido Island in the Latter Part of August, 1980, Geophysical Bulletin of Hokkaido University, Sapporo, Japan, Vol.40, pp.55−77, 1981. (in Japanese)

4. Scorer, R.S. : Theory of waves in the lee of mountains, Quart. J. Roy. Met. Soc., 75, pp.41−56, 1949.

5. Sarker, R.P. : Some modifications in a dynamical model of orographic rainfall, Mon. Wea. Rev., 95, pp. 673−684, 1967.

6. Colton, D.E. : Numerical simulation of the orographically induced precipitation distribution for use in hydrologic analysis, J. Appl. Met., 15, pp.1241−1251, 1976.

7. Tatehira, R. : Orographic rainfall computation including cloud− precipitation interaction, Tenki, 23, pp. 95−100, 1976. (in Japanese)

8. Sawyer, J.S. : A study of the rainfall of two synoptic situations, Quart. J. Roy. Met. Soc., 78, pp.231−246, 1952.

9. Sawyer, J.S. : The physical and dynamical problems of orographic rain, Quart. J. Roy. Met., 86, pp.326−345, 1956.

10. Gocho, Y. : Numerical Experiment of Orographic Heavy Rainfall due to a stratiform Cloud, Bull. Disaster Prevention Research Institute, Kyoto University, pp.405−422, 1978.

11. Kessler, E. : Models of mycrophysical parameters and processes, Meteorological Monographs, #10, pp.26−31, 1969.

12. Yamada, T.and Watanabe, H. : Analyses of Wind Field in Mountainous Areas, Proc. of JSCE, 43, pp.68−69, 1988. (in Japanese)

13. Yamada, T. and Watabe, G. : Numerical Simulation of Orographic Rainfall, Proc. of JSCE, 42, pp.98−99, 1987. (in Japanese)

14. Nakatsugawa, M., Yamada, T., Naitou, O. and Mizushima, T. : Simulation of Wind Field and Rainfall in Catchment Area, Proc. of the 33rd Japanese Conference on Hydraulics, pp.109−114, 1989. (in Japanese)